The Longitudinal Variation of Equatorial Waves due to Propagation on a Varying Zonal Flow

BRIAN J. HOSKINS

University of Reading, Reading, and Grantham Institute for Climate Change, Imperial College London, London, United Kingdom

GUI-YING YANG

National Centre for Atmospheric Science, and University of Reading, Reading, United Kingdom

ABSTRACT

The general 1D theory of waves propagating on a zonally varying flow is developed from basic wave theory, and equations are derived for the variation of wavenumber and energy along ray paths. Different categories of behavior are found, depending on the sign of the group velocity c_g and a wave property B. For B positive, the wave energy and the wavenumber vary in the same sense, with maxima in relative easterlies or westerlies, depending on the sign of c_g. Also the wave accumulation of Webster and Chang occurs where c_g goes to zero. However, for B negative, they behave in opposite senses and wave accumulation does not occur. The zonal propagation of the gravest equatorial waves is analyzed in detail using the theory. For nondispersive Kelvin waves, B reduces to 2, and an analytic solution is possible. For all the waves considered, B is positive, except for the westward-moving mixed Rossby–gravity (WMRG) wave, which can have negative B as well as positive B.

Comparison is made between the observed climatologies of the individual equatorial waves and the result of pure propagation on the climatological upper-tropospheric flow. The Kelvin wave distribution is in remarkable agreement, considering the approximations made. Some aspects of the WMRG and Rossby wave distributions are also in qualitative agreement. However, the observed maxima in these waves in the winter westerlies in the eastern Pacific and Atlantic Oceans are generally not in accord with the theory. This is consistent with the importance of the sources of equatorial waves in these westerly duct regions due to higher-latitude wave activity.

1. Introduction

A number of observational and theoretical studies have discussed the significant effect of the ambient zonal flow on equatorial wave behavior (e.g., Webster and Holton 1982; Webster and Chang 1988; Zhang 1993; Tomas and Webster 1994; Chang and Webster 1995; Hoskins and Yang 2000; Yang et al. 2007a,b,c, 2011, 2012; Dias and Kiladis 2014). Yang and Hoskins (2013) showed that tropical ENSO-related variation of the zonal flow can lead to variations of equatorial Kelvin wave activity, and Yang and Hoskins (2015, manuscript submitted to *Quart. J. Roy. Meteor. Soc.*) shows this also for $n = 0$ mixed Rossby–gravity and $n = 1$ Rossby waves. These two studies use ENSO as a test bed for understanding the impact of the zonal flow variation in equatorial waves. Three mechanisms for zonal flow impact are given in Yang and Hoskins (2015, manuscript submitted to *Quart. J. Roy. Meteor. Soc.*): that the zonal flow variation can determine 1) the possible existence of free waves, 2) the likely response to forcing, and 3) the zonal propagation of equatorial wave activity. In that study, the focus is on the variation of wave forcing associated with ENSO variation as well as on the first two mechanisms.

The third mechanism has been investigated in a number of studies (e.g., Bretherton and Garrett 1968; Webster and Chang 1988). Webster and Chang (1988) considered the change in energy following an equatorial wave propagating in a zonally varying basic state and

introduced and stressed the importance of wave accumulation but did not give a complete, explicit expression for energy change for equatorial waves. Here we will explore such an expression for energy and for other changes in wave properties along the ray paths of all equatorial waves and will briefly examine its relevance to observed behavior.

Section 2 will give the general theory for 1D propagation in a slowly varying zonal flow. Section 3 will introduce the different categories of possible wave behavior and show schematics of their behavior. In section 4 the general theory is applied to equatorial waves in the real tropospheric atmosphere winter, with the detailed mathematical derivations for each wave being given in the appendix. The relevance of the theory to observed wave climatologies in winter and summer is discussed in section 5 and concluding comments are given in section 6.

2. Variation of wave properties in zonal propagation

The analysis in this section closely follows the general form given in Lighthill (1978, chapters 4.5 and 4.6). We consider waves on a zonal flow $U(x)$ and assume that it is slowly varying such that the waves are merely Doppler shifted by the zonal flow. Hence for any wave mode the absolute frequency ω is given by

$$\omega = U(x)k + \omega_i(k), \qquad (1)$$

where k is the zonal wavenumber and i stands for intrinsic (i.e., the property in a resting atmosphere). For convenience, we will take k to be positive and allow ω and ω_i to take either sign. The zonal group velocity is

$$c_g = \partial\omega/\partial k = U + c_{gi}, \qquad (2)$$

where $c_{gi} = \partial\omega_i/\partial k$. Defining $(d/dt)|_r$ to be the time derivative moving along a ray path, the coordinate of the position on the ray path changes according to

$$\left.\frac{d}{dt}\right|_r x = c_g. \qquad (3)$$

There is no explicit time dependence on the right-hand side of Eq. (1), which means that

$$\left.\frac{d}{dt}\right|_r \omega = 0, \qquad (4)$$

so that the frequency is constant along a ray path. The explicit x dependence on the right-hand side of Eq. (1) is only through the term $U(x)k$, and so, following Lighthill (1978),

$$\left.\frac{d}{dt}\right|_r k = -k\frac{dU}{dx}. \qquad (5)$$

Equation (5) is a special case of Eq. (106) in Lighthill (1978).

From Eqs. (1), (4), and (5),

$$\left.\frac{d}{dt}\right|_r \omega_i = -\left.\frac{d}{dt}\right|_r (Uk) = -c_g k\frac{dU}{dx} - U\left.\frac{d}{dt}\right|_r k$$

$$= -c_g k\frac{dU}{dx} + Uk\frac{dU}{dx} \quad \text{or}$$

$$\left.\frac{d}{dt}\right|_r \omega_i = -c_{gi} k\frac{dU}{dx}. \qquad (6)$$

The change in wave energy density E along a ray path is determined through consideration of the wave action density, $\xi = E/\omega_i$, which in a slowly varying state satisfies a conservation equation [e.g., Bretherton and Garrett 1968; Lighthill 1978, his Eq. (162)]:

$$\frac{\partial\xi}{\partial t} + \frac{\partial(c_g\xi)}{\partial x} = 0 \quad \text{or}$$

$$\left.\frac{d}{dt}\right|_r \xi = -\xi\frac{\partial c_g}{\partial x}. \qquad (7)$$

Along a specific ray, ω is constant but k, ω_i, and c_g change with U and, therefore, with position $x(t)$. The change in wave energy E along a specific ray is given by Eq. (7):

$$\left.\frac{d}{dt}\right|_r \frac{E}{\omega_i} = -\frac{E}{\omega_i}\frac{dc_g}{dx} \quad \text{or} \quad \frac{1}{\omega_i}\left.\frac{d}{dt}\right|_r E - \frac{E}{\omega_i^2}\left.\frac{d}{dt}\right|_r \omega_i = -\frac{E}{\omega_i}\frac{dc_g}{dx}.$$

Using Eq. (6), this becomes

$$\left.\frac{d}{dt}\right|_r E = \frac{E}{\omega_i}\left(-kc_{gi}\frac{dU}{dx}\right) - E\left(\frac{dc_{gi}}{dx} + \frac{dU}{dx}\right)$$

$$= -E\left[\left(\frac{kc_{gi}}{\omega_i} + 1\right)\frac{dU}{dx} + \frac{dc_{gi}}{dx}\right]. \qquad (8)$$

But on a specific ray,

$$\frac{dc_{gi}}{dx} = \frac{dc_{gi}}{dk}\frac{dk}{dx},$$

and Eq. (5) gives

$$c_g dk/dx = -k dU/dx.$$

Therefore, Eq. (8) can be written

$$\left.\frac{d}{dt}\right|_r E = -BE\frac{dU}{dx}, \qquad (9)$$

where

$$B = 1 + \frac{c_{gi}}{c_i} - \frac{k}{c_g}\frac{\partial c_{gi}}{\partial k}, \qquad (10)$$

where c_i is the intrinsic phase speed. Equations (4), (6), (5), and (9) give the change along a ray path of, respectively, the absolute and intrinsic frequencies, wavenumber, and energy. The first of these gives that the absolute frequency is constant and the other three may be rewritten:

$$\left.\frac{d}{dt}\right|_r \ln|\omega_i| = -\frac{c_{gi}}{c_i}\frac{dU}{dx}, \qquad (11)$$

$$\left.\frac{d}{dt}\right|_r \ln k = -\frac{dU}{dx}, \quad \text{and} \qquad (12)$$

$$\left.\frac{d}{dt}\right|_r \ln E = -B\frac{dU}{dx}. \qquad (13)$$

The rates of change along a ray of the logarithms of the intrinsic frequency, wavenumber, and energy are proportional to the convergence of the zonal flow. For the intrinsic frequency and the energy, the proportionality is through terms that depend on the properties of the waves under consideration.

Because the frequency is conserved along a ray path, any ray can be referred to by the frequency or period of the particular wave and the starting point of the ray. Along such a ray,

$$\left.\frac{d}{dt}\right|_r = c_g\frac{d}{dx},$$

and so the wavenumber and energy equations, Eqs. (12) and (13), become

$$\frac{d\ln k}{dx} = -\frac{1}{c_g}\frac{dU}{dx} \quad \text{and} \qquad (14)$$

$$\frac{d\ln E}{dx} = -\frac{B}{c_g}\frac{dU}{dx} \qquad (15)$$

For steady-state distributions of a particular wave, we can consider the distribution with longitude of wave properties given by Eq. (14) together with the dispersion relation and the wave energy given by Eq. (15). The triggering of the waves could be at any point in longitude, with the interest being on the subsequent wave properties as a function of longitude in the direction of the group velocity. However, if wave triggering in extended regions dominates, then these distributions are likely to have little similarity with those observed.

3. Interpretation of the wave properties in a steady state

In this section, the behavior of the steady-state wave properties, particularly the wavenumber and energy

density, will be interpreted. The relevant equations are Eqs. (14) and (15) with Eq. (10).

Consider first the wavenumber, as given by Eq. (14). The sense of the change in $\ln k$ with x depends on the sign of c_g, and the magnitude of the change varies inversely with the magnitude of c_g. For simplicity in this section, we make the reasonable assumption that in $c_g = U + c_{gi}$ the variation of U dominates and that c_g increases or decreases with x in the same sense as U. In particular, for the schematic examples the variation in c_{gi} is neglected, and the variation in c_g is taken to be equal to that in U (this is strictly true only for nondispersive waves). In this case, the right-hand side of Eq. (14) may be written as $d/dx(\ln|U + c_{gi}|)$ and so

$$k = k_0\left|\frac{U_0 + c_{gi}}{U + c_{gi}}\right| = k_0\left|\frac{U_0 + c_{gi}}{c_g}\right|, \qquad (16)$$

where k_0 is the zonal wavenumber at a longitude at which $U = U_0$. If the wave frequency is specified, then k_0 would be determined here from the dispersion relation.

Figure 1 shows schematics for the behavior of k for a steady state with waves propagating on a simple sinusoidal basic flow, which is indicated in the left-hand column. Any constant can be added to this flow with no difference to the results: it is its zonal variation that matters, but the minimum zonal flow region will be referred to as easterlies and the maximum as westerlies, consistent with the general situation found in the equatorial upper troposphere. Schematics of E and k are given in columns 2–5 for a range of values of B: −1, 0, 1, and 2, respectively. The plots in rows 1–4 and columns 2–5 are therefore arranged with B as the abscissa and c_g as the ordinate.

For c_g positive at all longitudes the waves are able to propagate around Earth. This case, "P" (standing for positive everywhere), is shown in the top row in Fig. 1. It is clear from Eq. (14) that the zonal variation of $\ln k$, and therefore of k, is in the opposite sense to that of U. Also, because of the inverse c_g dependence, the minimum in the westerlies is rather flat and the maximum in the easterlies is more peaked than a sinusoid. Note that k is not dependent on B and is shown by a dotted line in columns 2–5. If c_g is mostly positive, referred to as "p," but zero either side of the easterly maximum, as shown in the second row in Fig. 1, then eastward-propagating waves cannot penetrate the negative c_g region and the wavenumber tends to infinity as the waves approach the zero c_g point on the western flank of the easterlies. This means that the wavelength becomes shorter and shorter as the waves propagate in from the west at an ever smaller group velocity. Also in the negative c_g regions,
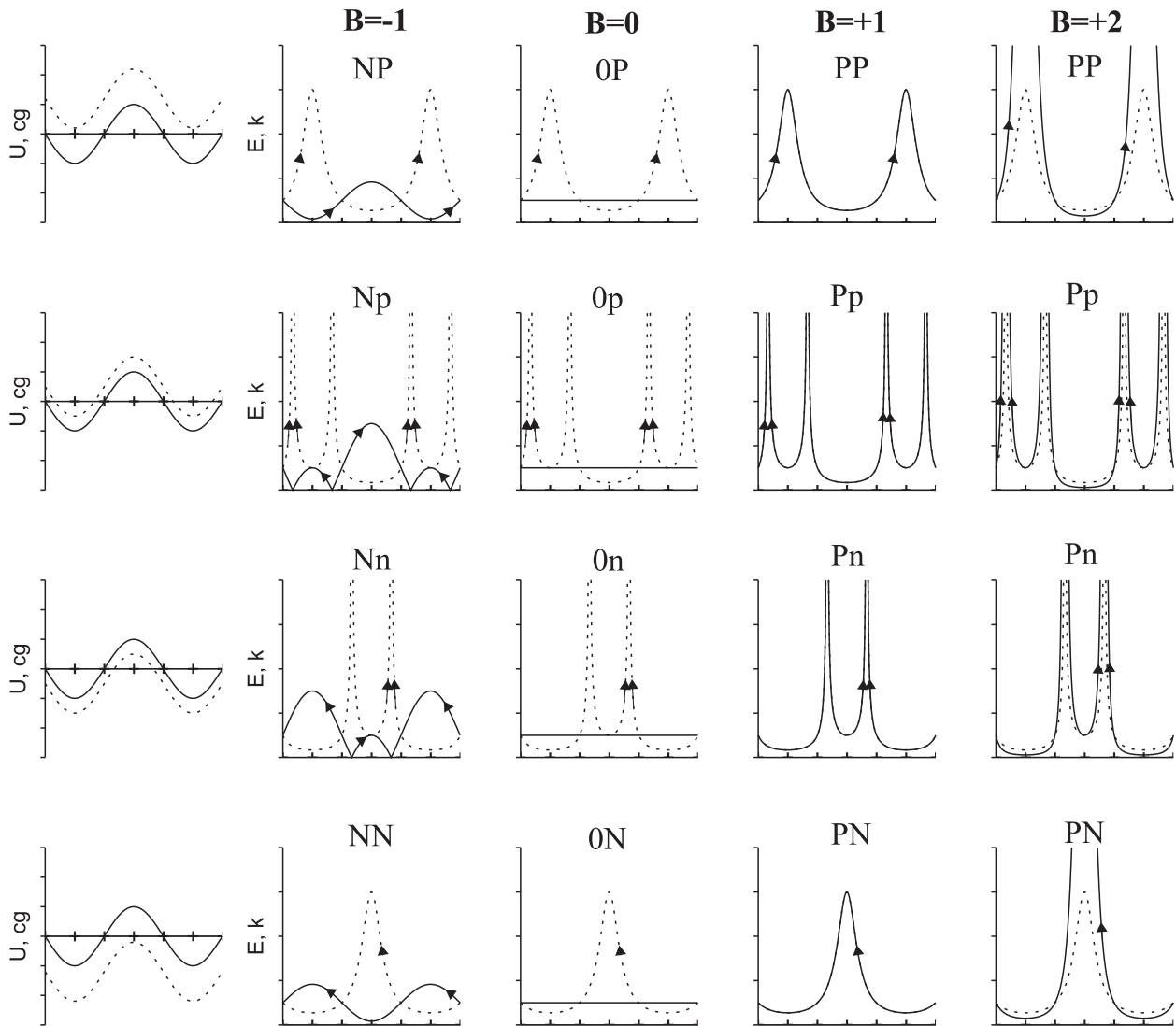
FIG. 1. Schematics of the longitudinal variation of (column 1) ambient zonal wind U (solid) and group velocity c_g (dotted) and (columns 2–5) E (solid) and k (dotted) for specified U and c_g and the wave property B [defined in Eq. (10)]. For the cases illustrated, U is zonal wavenumber 1, and the longitude region 0°–180° is repeated on the right-hand side for clarity. The tick marks on the abscissas are drawn every 90°. Note that U is the same sinusoidal wind in all cases and the tick mark interval on the ordinates has the magnitude of U; c_g is taken to vary in longitude as U but is offset by (top to bottom) 1.2, 0.5, −0.5, and −1.2 times U, respectively. For the upper troposphere the amplitude of U and the tick mark interval could be taken to be $10 \, \mathrm{m \, s^{-1}}$. Columns 2–5 show schematics of E and k for $B = -1, 0, +1$, and +2, respectively. Therefore, B increases from left to right and c_g increases from the bottom to the top. As described in the text, each case is categorized by the two letters at the top, with the first letter corresponding to the sign of B (positive, zero, or negative) and the second letter corresponding to the sign of c_g. The arrows indicate the direction of the group velocity and are placed where the values of E and k are increasing following the rays.

similar behavior occurs as the waves propagate toward the same points from the east.

The case c_g mostly negative, referred to as "n" is shown in the third row of Fig. 1. This is like the "p" case in the second row, but the zero c_g, infinite k point is now on the eastern flank of the westerlies. The fourth row in Fig. 1 shows the case when c_g is negative throughout, referred to as "N." Here the variation of k is in the same

sense as U, with a rather flat minimum in the easterlies and a sharper peak in the westerlies.

For wave energy and Eq. (15), the considerations are similar but now the wave factor B has to be considered. Looking at Eq. (10), it is clear that for a nondispersive wave, the second term is equal to one and the third term is zero. Therefore, $B = 2$. More generally, term 2 in B is positive or negative according to whether c_i and c_{gi} have

the same or opposite signs. Term 3 depends on the absolute group velocity and the change in intrinsic group velocity with wavenumber and can have either sign. This term has a singularity at zero absolute group velocity.

It is clear that B will in general vary with k and U and could have either sign, though positive is more likely. However it is convenient for an initial discussion to neglect the variation of B as well as that of c_{gi}. In this case, Eq. (15) can be solved to give

$$E = E_0 \left| \frac{U_0 + c_{gi}}{U + c_{gi}} \right|^B = E_0 \left| \frac{U_{0+} c_{gi}}{c_g} \right|^B. \quad (17)$$

Here E_0 is an arbitrary amplitude at the longitude at which $U = U_0$; the focus here is on how the energy varies with the local velocity. Then if B is a positive constant, the behavior will be like that of the wavenumber, and it will be identical if $B = 1$. In Fig. 1, this value is used in the fourth column. The panels in this column show E for positive ("P"), mostly positive ("p"), mostly negative ("n"), and negative ("N") c_g, respectively, from rows 1 to 4. If B is greater than one, as in the fifth column, then the large c_g minima are even flatter and the small c_g maxima are even sharper than for k. For B less than one the minima with be less flat and the maxima less sharp than those of k, and for B equal to zero, as in the third column, the energy distribution is independent of position.

Therefore, for B positive ("P") and c_g positive ("P"), referred to as category PP and shown in columns 4 and 5, row 1, large wave energy is expected in the easterlies. For B positive and c_g mostly positive (category Pp, columns 4 and 5, row 2), energy as well as wavenumber tends to infinity at the zero c_g point on the western flank of the easterlies. This is referred to by Chang and Webster (1995) as energy accumulation. For B positive and c_g mostly negative (case Pn, columns 4 and 5, row 3) wave energy accumulates on the eastern flank of the westerlies. For B positive and c_g negative (case PN, columns 4 and 5, row 4) wave energy is maximum in the westerlies.

As stated above, for $B = 0$ (column 3) E does not change with position. For B negative ("N") the wave energy and wavenumber behave in opposite senses and the behavior is very different from positive B. This is illustrated in the second column of Fig. 1, where B is again taken to be constant, this time −1. For c_g positive everywhere (case NP in column 2, row 1), the wave energy now varies in the same sense as the zonal flow and opposite to the wavenumber: the energy peaks in the westerlies and has a minimum in the easterlies. If c_g has zeros on either flank of the easterlies (case Np,

column 2, row 2), then E is again a maximum in the westerlies. However, at the zero c_g points on the western flank of the easterlies, $\ln E$ tends to minus infinity and E goes to zero as the wave propagates ever more slowly toward them. For c_g mainly negative (case Nn, column 2, row 3) and negative everywhere (case NN, column 2, row 4) the dominant wave energy maximum is now in the easterlies.

For B negative, the c_g^{-1} factor in it [see Eq. (10)] tends to decrease the difference between the peaks and the troughs in the energy. This contrasts with the positive B case in which it amplified the differences. It should also be noted that the negative B case differs markedly from the positive B case in its behavior near-zero group velocity points. The wave energy goes toward zero rather than toward infinity, and the concept of wave energy accumulation does not apply, despite the fact that the wavenumber tends to infinity and the wavelength shrinks to zero.

4. Application to equatorial waves

In this section the general theory developed in section 2 is applied to equatorially trapped waves. We will consider two 6-month seasons, November–April and May–October, for convenience, referred to as winter and summer. The different classes of waves will be discussed in separate subsections below, but for reference Fig. 2 contains a summary of the dominant behavior of the waves in terms of typical magnitudes of c_g and B and the categories illustrated schematically in Fig. 1. The detailed mathematical derivations for each wave are given in the appendix, and the focus here is on the possible implications for the propagation of equatorial waves on zonal flows like those in the upper troposphere. For illustration, the equivalent depth h_e is generally chosen to be 40 m, corresponding to a gravity wave speed $[c_e = (gh_e)^{1/2}]$ of 20 m s^{-1}. However, it is shown that westward-moving mixed Rossby–gravity waves and Rossby waves in the Western Hemisphere in winter have a more barotropic structure (e.g., Kiladis and Wheeler 1995; Yang et al. 2007a, 2011, 2012; Yang and Hoskins 2015, manuscript submitted to *Quart. J. Roy. Meteor. Soc.*), so $h_e = 200$ m and gravity wave speed of 44 m s^{-1} are usually used there for these waves.

a. Kelvin waves

Kelvin waves are nondispersive. Therefore, $B = 2$, and the steady wave field solutions for k and E given in Eqs. (16) and (17) are exact with this value for B. For any realistic equivalent depth, the Kelvin wave speed $c_i = (gh_e)^{1/2}$ is large enough compared with the easterly winds in the troposphere that c_g is always positive and
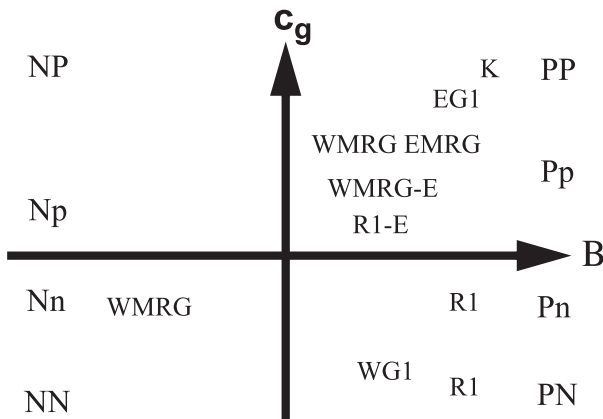
FIG. 2. A summary of equatorial wave behavior categories in terms of their typical values of B and c_g and of the basic categories shown schematically in Fig. 1. Only the dominant behavior in the upper troposphere is shown. The names for the waves are as defined in section 3. WMRG is shown in category Pp for westerly winds and low wavenumbers and in category Nn for easterly winds. WMRG-E is shown in category Pp for westerly winds and high wavenumbers. R1 is shown in categories Pn and PN for easterly winds and also for westerly winds and low wavenumber. R1-E is shown in category Pp for westerly winds and high wavenumbers.

this is an example of case PP in Fig. 1. Figure 3 shows the k and E solutions for a smoothed version of the equatorial upper-tropospheric zonal wind in winter and summer for various wave periods (and therefore various k_0). Both k and E show longitudinal variation that is the inverse of that of the zonal flow, with maxima in relative easterlies and minima in relative westerlies, as expected in category PP. The peaks are sharper and the minima flatter in E corresponding to the factor 2 in Eq. (15) and the related square on the right-hand side of Eq. (17).

Figures 4a and 5a show B and B/c_g, respectively (colors), for Kelvin waves as a function of wavenumber and zonal flow speed. Also shown in the figures are lines of constant frequency ω (black) and group velocity, c_g (white). Positive ω contours (solid) correspond to eastward-moving waves and negative contours to westward-moving waves. In the case of the nondispersive Kelvin wave, many of the variables have a simple distribution. Since ω is constant along a ray path, such a path would correspond to moving along an ω contour according to the changing zonal wind. The thick line segments correspond to ray paths for tropospherically relevant values with a zonal wind varying between -10 and $+17\,\mathrm{m\,s}^{-1}$ and periods of 40, 10, and 5 days, as shown in Fig. 3. The changing zonal wavenumber along a ray path is indicated by the changing abscissa.

b. Eastward-moving mixed Rossby–gravity waves

For the gravity wave–like, $n = 0$, eastward-moving mixed Rossby–gravity wave (EMRG), B and B/c_g are

shown in Figs. 4b and 5b. Note that B is positive almost everywhere, with values typically between 1 and 2. As c_g goes to zero (white dashed line), there is a discontinuity in B and on its high-frequency side a narrow region of negative values. This is not, in general, relevant for the troposphere in winter but may be relevant for summer when the easterlies are stronger and also in the stratosphere. For the EMRG, c_g is positive for periods shorter than about 3 days and B/c_g is positive (Fig. 4b). Therefore, in general, the EMRG is also in category PP in Fig. 1, so that maximum wave energy and wavenumber are predicted in relative easterly peaks and minima in relative westerly peaks. However, for strong easterly winds such as in the eastern hemisphere in summer and lower frequencies, the EMRG can be in categories PN or Pn, with maxima in or on the eastern flank of the weakest easterlies.

c. Gravity waves

The $n = 1$ eastward-moving gravity wave (EG1) has patterns of B and B/c_g (Figs. 4c and 5c) quite similar to those of the EMRG, with B positive except near the zero c_g line and typical values now in the range 0.5–1.5. For periods shorter than 2 days, c_g is positive. It is negative only for longer periods, low wavenumbers, and strong easterly winds. Therefore, the EG1 is generally again in category PP. However, category PN is relevant for strong easterly winds and low wavenumbers, with large energy and wavenumber values near minima in the strong easterly winds.

The $n = 1$ westward-moving gravity wave (WG1) has a distribution of B (Fig. 4d) that is similar to that of EG1 but reflected in the x axis. However, over most of the domain c_g is negative so that B/c_g is negative (Fig. 5d). Therefore, the WG1 is generally in category PN, with maximum wave energy and wavenumber in westerly flow maxima. However, for long periods, low wavenumbers, and strong westerly flows c_g is positive and the WG1 would be in category PP, with wave energy maximizing in westerly flow minima.

d. Westward-moving mixed Rossby–gravity waves

For the Rossby wave–like, $n = 0$, westward-moving mixed Rossby–gravity wave (WMRG), B and B/c_g are shown in Figs. 4e and 5e for $h_e = 40$ m and Figs. 4g and 5g for $h_e = 200$ m. The former is seen as relevant to the Eastern Hemisphere (EH) and the latter to the Western Hemisphere (WH). Because the upper-tropospheric winds are mostly easterly in the former and westerly in the latter, it is the lower half of the domain in the 40-m case and the upper half of the domain in the 200-m case that are most relevant here. In fact, there is much similarity between the pictures for the two depths. For both
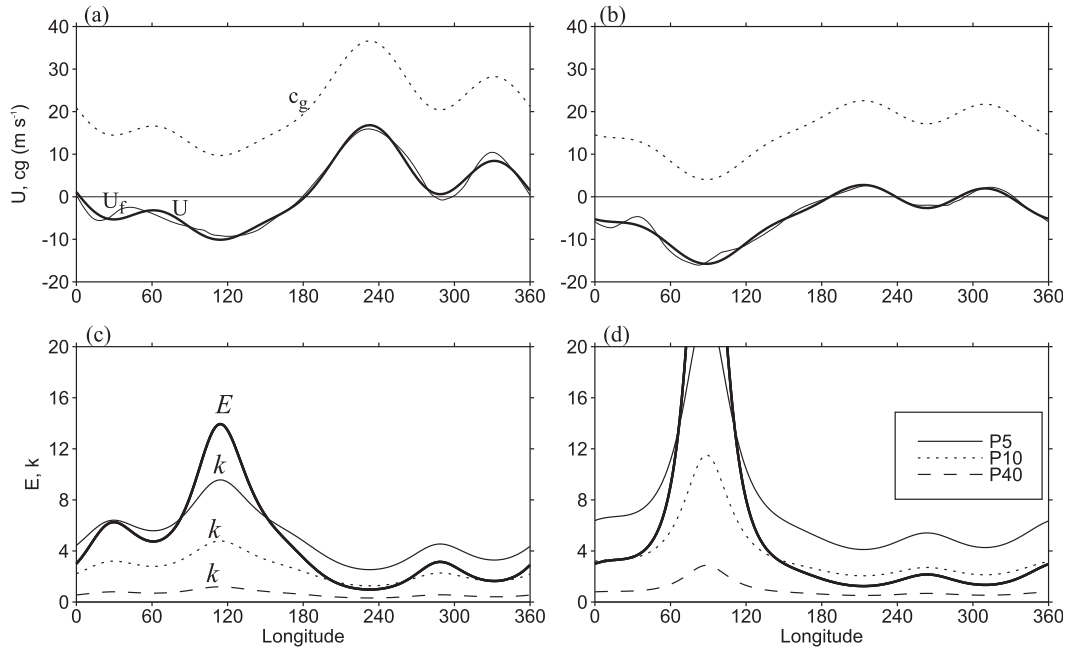
FIG. 3. Equatorial zonal wind and Kelvin wave steady-state wavenumber k and wave energy E for (a),(c) winter and (b),(d) summer. The climatological zonal wind averaged between 7°N and 7°S and from 250 to 150 hPa is shown in (a) and (b) (light solid line) along with a smoothed version (zonal wavenumbers 0–4, thick solid line). The implied Doppler-shifted velocity (using $h_e = 40\,\mathrm{m}$) is also shown (dotted line). In (c) and (d) the steady-state solutions for E are shown (thick solid line). The solutions for k are also shown for periods 5 (thin solid line), 10 (dotted line), and 40 days (dashed line).

depths, B is positive, typically from 0.5 to 2, for westerlies and for weak easterlies and low wavenumbers, but mainly negative, typically from -0.2 to -1, in easterlies stronger than about $5\,\mathrm{m\,s^{-1}}$. For the 40-m depth, a typical WMRG wave in easterlies with a period 3 days (as indicated) would have negative c_g also. Therefore, it would be in category NN and have maximum wave energy and minimum wavenumber in easterly maxima. Low wavenumbers in both easterlies (considering $h_e = 40\,\mathrm{m}$) and westerlies (considering $h_e = 200\,\mathrm{m}$) have negative frequency (westward moving), positive c_g and B, so that they are in category Pp or PP, with wave energy and wavenumber maxima at zero zonal flow and c_g points or in westerly minima. Low wavenumber WMRG would be able to propagate eastward from stronger westerlies into weak westerlies or even easterlies. They would accumulate, but for those frequency curves crossing the zero c_g line, such as that with $h_e = 200\,\mathrm{m}$ and a 3-day period (Fig. 4g), there would be a small overshoot and reversal in eastward propagation before this occurred.

For stronger westerly flow and shorter wavelengths (Figs. 4g and 5g), the frequencies are positive, implying Doppler-shifted eastward movement. In Yang and Hoskins (2015, manuscript submitted to *Quart. J. Roy. Meteor. Soc.*), where this is discussed in more detail, these waves with WMRG structure but eastward movement

are referred to as WMRG-E. Like the low-wavenumber WMRG in westerlies, the WMRG-E waves are in category Pp. WMRG-E waves only exist in westerlies and as they propagate eastward from maximum westerlies toward weak westerlies, the group velocity decreases toward zero, and the wavenumber and energy increase.

We will now discuss some examples of ray tracing that will illustrate the most important range of behavior of MRG waves relevant to the upper troposphere. The equations used are the full ray equations, Eqs. (2), (12), and (13), with B [Eq. (10)] and c_g determined from the full dispersion relation (see the appendix). The background zonal wind (Fig. 6a) is the same as used for Kelvin wave calculation (Fig. 3a). We choose h_e to be 40 or 200 m for rays starting in the EH or WH, respectively. The starting points are 120°, 210°, and 330°E and the periods are 3 and 10 days. Rays are continued 30° into the other hemisphere where the alternative equivalent depth would be more applicable and then they are stopped. WMRG and WMRG-E waves are shown by black and gray lines, respectively, and the associated segments of the frequency contours are highlighted in the MRG panels in Figs. 4e,g and 5e,g.

Starting at 120°, there is a 3-day WMRG propagating westward (black line) and a 3-day EMRG (thick gray line) propagating eastward (Figs. 6b,c). The numbers 1,
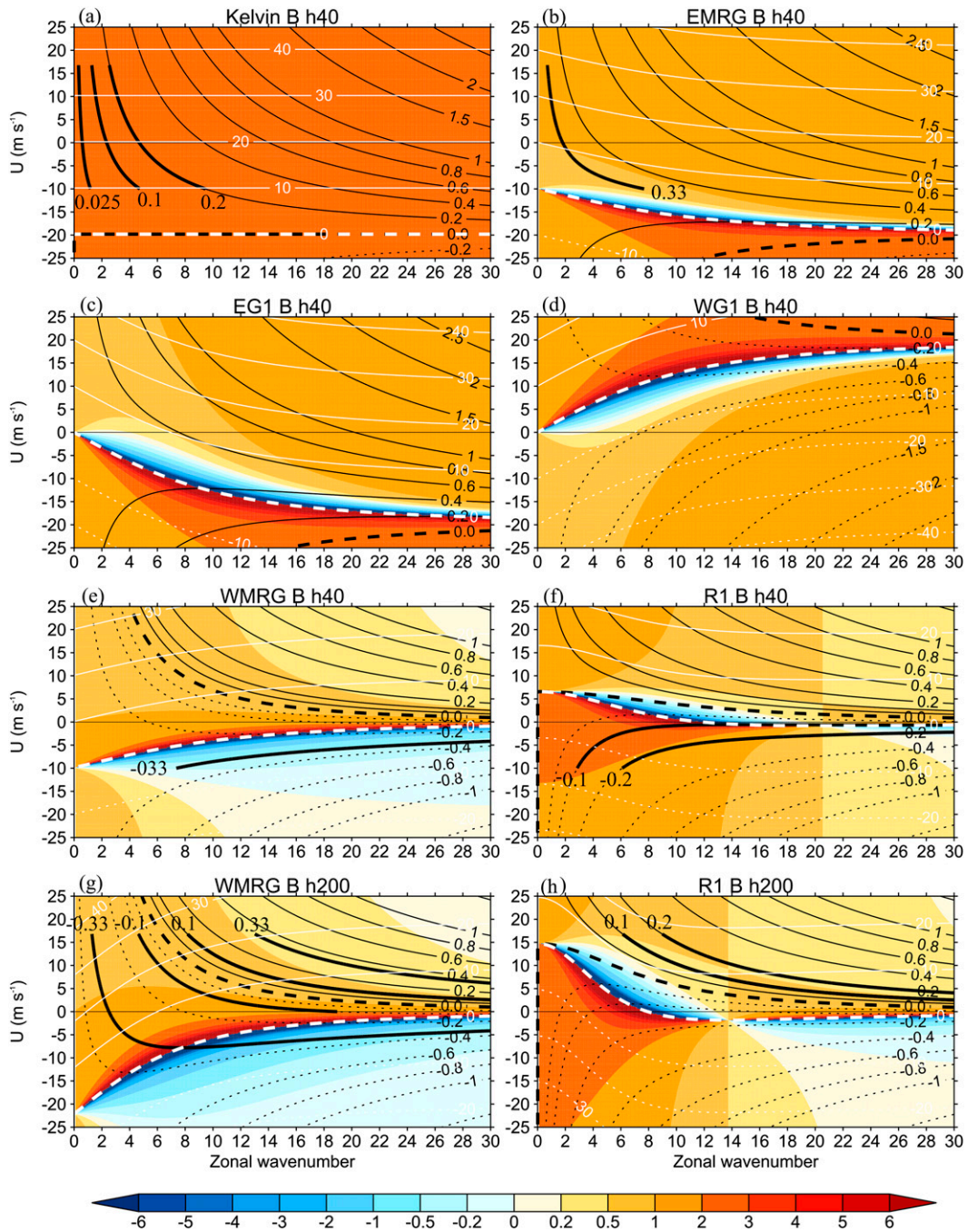
FIG. 4. Wave property B (color) as a function of zonal wavenumber and ambient zonal wind U, with B defined in Eq. (10) for (a) the Kelvin, (b) EMRG, (c) EG1, (d) WG1, (e) WMRG, and (f) R1 waves with $h_e = 40$ m. (g),(h) WMRG and R1, respectively, with $h_e = 200$ m. The black lines are for Doppler-shifted frequencies ω (cpd) and white lines are for group velocity (m s^{-1}). The positive contours are solid, the zero contour is dashed, and negative contours are dotted. For the group velocity zero contour, the dashed line is thicker. A few thick black lines with a constant frequency values show various ray paths for which calculations are shown in Figs. 6 and 7. For ω, the contour interval is 0.2 for $|\omega| < 1$ and 0.5 for $|\omega| \geq 1$. For WMRG and R1, $\omega = \pm 0.05$ and ± 0.1 are also shown but not labeled. The contour interval for c_g is 10.
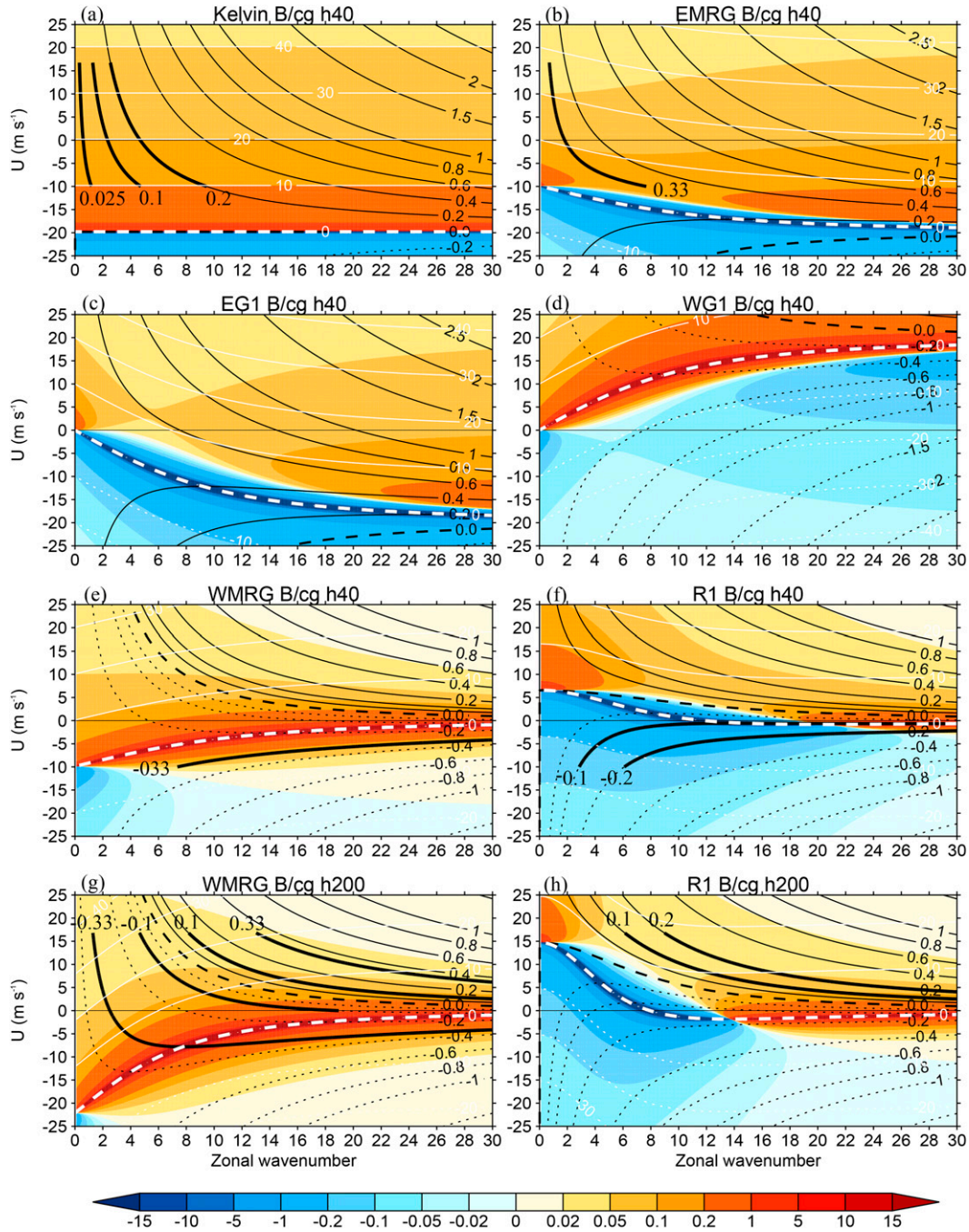
FIG. 5. As in Fig. 4, but for B/c_g.

2, and 3 indicate their positions after 10, 20, and 30 days, respectively. The WMRG exhibits a slight decrease in the magnitude of the westward group velocity up to about day 20 (Fig. 6c). Associated with this are a sharp increase in wavenumber (Fig. 6d) and a decrease in wave energy (Fig. 6e). This behavior, with energy decrease rather than accumulation, is consistent with the wave being in category NN. The EMRG has a large and

increasing eastward phase speed (Fig. 6b) and an eastward group velocity increasing in sympathy with the ambient flow (Fig. 6c). At the same time, its wavenumber (Fig. 6d) and wave energy (Fig. 6e) decrease, consistent with it being in category PP.

For the chosen periods of 3 and 10 days, four waves are possible at 210°E, both WMRG and WMRG-E, each with both periods (Fig. 6b). All four have eastward
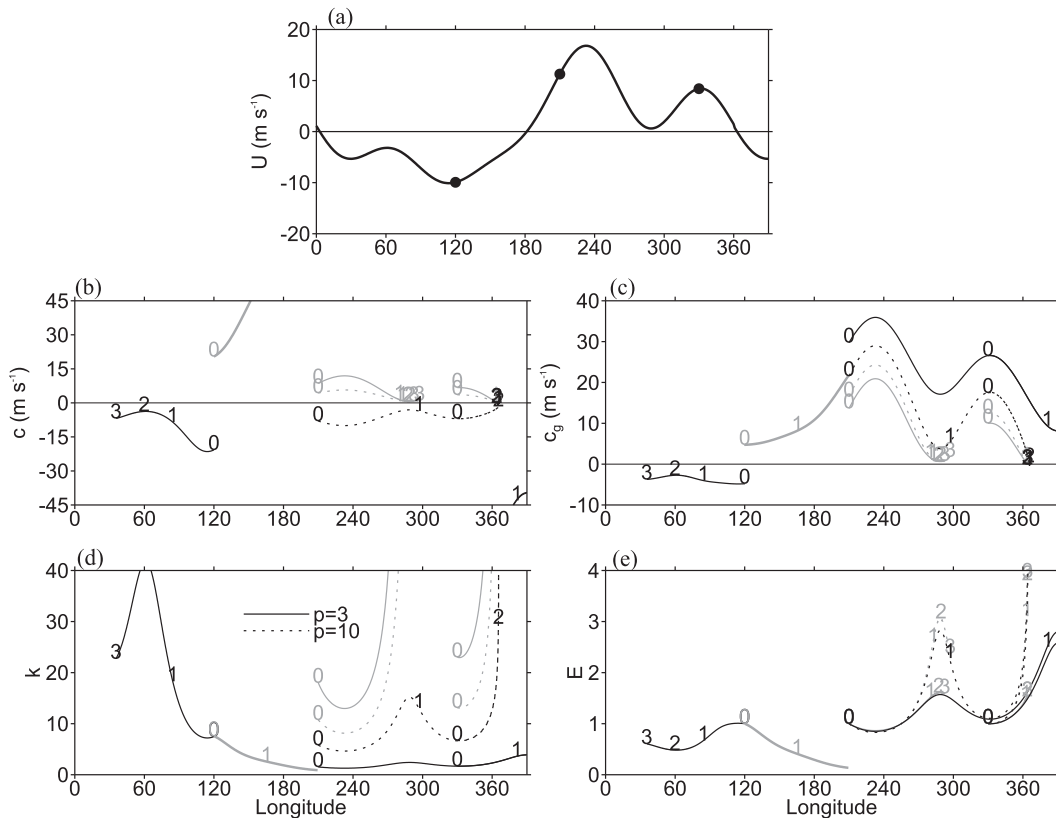
FIG. 6. Ray-tracing results for MRG waves on the smoothed upper-tropospheric winter zonal flow. (a) Zonal flow, (b) phase speed, (c) group velocity, (d) wavenumber, and (e) wave energy. The starting points for the rays are 120°, 210°, and 330°E, indicated by the solid cycle in (a), and the periods are 3 (solid) and 10 days (dotted). For rays starting in the EH, $h_e = 40$ m throughout. For rays starting in the WH, $h_e = 200$ m throughout. For the rays with positive phase speed, EMRG and WMRG-E are shown by thick and thin gray lines, respectively. The rays are followed for 30 days in general, with the numbers 0, 1, 2, and 3 indicating days 0, 10, 20, and 30, respectively. However, the EMRG is terminated at 210°E, and the domain is continued on the right-hand side to 390° to show the behavior of some WH waves.

group velocities (Fig. 6c), which change in sympathy with the ambient flow. The group velocities are smaller for the WMRG-E waves and as they propagate toward the near-zero flow between the eastern Pacific (E Pacific) and Atlantic westerlies, their group velocities become very small. The wavenumbers (Fig. 6d) and wave energy (Fig. 6e) of all four waves reach a minimum in the eastern Pacific westerly maximum and then increase as the group velocity decreases. At the point of the minimum westerlies, the WMRG-E waves have large energy and wavenumber. Waves initiated in the Atlantic westerlies at 330°E behave similarly. The behavior of the WMRG waves is characteristic of category PP and that by the WMRG-E waves category Pp.

e. n = 1 Rossby wave

For the $n = 1$ Rossby wave (R1) B and B/c_g are shown in Figs. 4f and 5f for $h_e = 40$ m and Figs. 4h and 5h for $h_e = 200$ m. In both cases, B is positive, typically from 0.5

to 3, except in a narrow band close to the zero c_g line. Considering easterly flow and $h_e = 40$m (Figs. 4f and 5f), R1 waves have positive B and negative c_g so that in a flow where the easterlies become westerlies they are in category Pn: the wavenumber and energy are unbounded as the waves approach a zero in c_g. For a flow that is easterly everywhere, R1 waves are in category PN with maxima in wavenumber and energy in minimum easterlies. For weak westerly flow and $h_e = 200$ m, low wavenumbers have a westward group as well as phase speed, so that they also have category Pn behavior, though as the frequency curve crosses the zero c_g line, they overshoot slightly as they accumulate. In Figs. 4h and 5h, there is a narrow band of negative B in westerlies with c_g positive and low frequency, indicating that the R1 waves there can be in category Np, with maximum energy and minimum wavenumber in westerly maxima.

For stronger westerlies and higher wavenumbers (see Figs. 4h and 5h), the R1 wave structure is Doppler
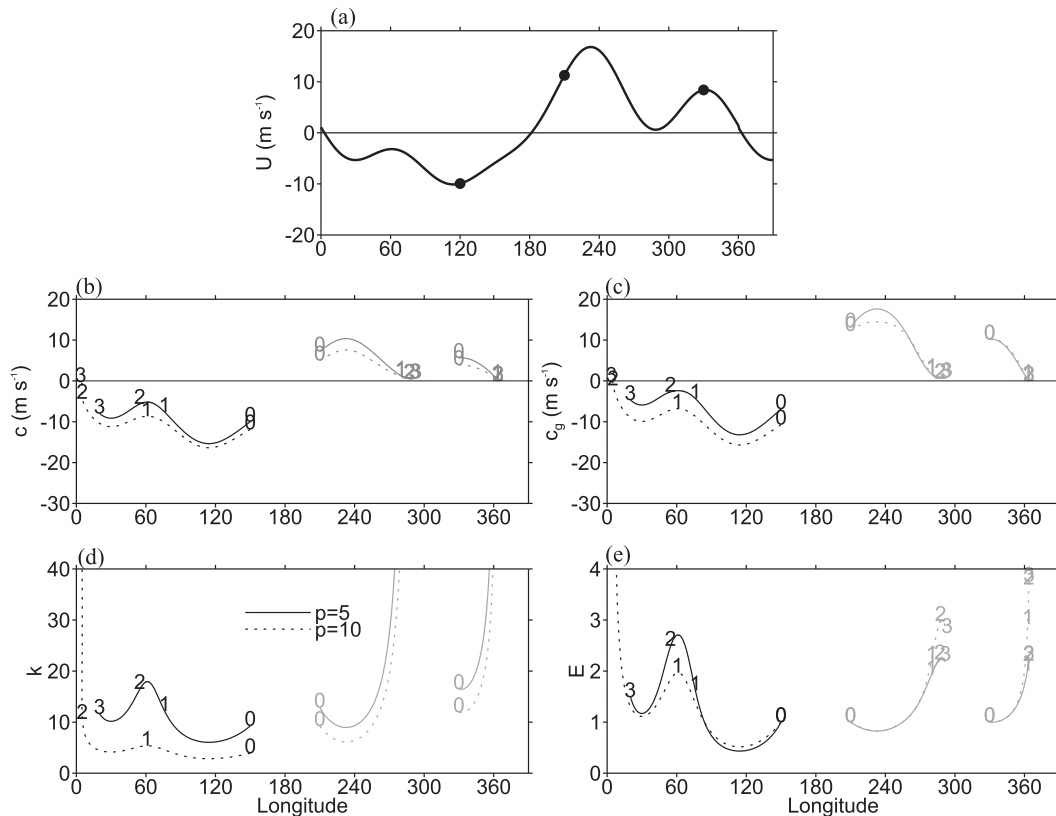
FIG. 7. Ray-tracing results for R1 waves on the smoothed upper-tropospheric winter zonal flow. As in Fig. 6, except that the periods are 5 (solid) and 10 days (dotted) and the starting points are 150°, 210°, and 330°E, and gray lines are for R1-E.

shifted to move eastward, and as in Yang and Hoskins (2015, manuscript submitted to *Quart. J. Roy. Meteor. Soc.*) the waves are termed R1-E. They have both B and c_g positive and are in category Pp, accumulating with unbounded wave energy and wavenumber at zero-wind points where their c_g is also zero.

As was done for MRG waves, some illustrative ray tracing is now presented for R1 waves (Fig. 7). The conditions are the same as used before except that the initiation points are now 150°, 210°, and 330°E and the periods are 5 and 10 days. The associated segments of the frequency contours are highlighted in the R1 panels in Figs. 4f,h and 5f,h. In the easterlies at 150°E there are westward-moving R1 waves with both these periods (Fig. 7b). Both show group velocities (Fig. 7c) that change in sympathy with the zonal flow and wavenumbers (Fig. 7d) and energies (Fig. 7e) that reach minima in the stronger easterlies near 110°E, maxima in the weaker easterlies near 60°E, and a minimum in the stronger easterlies near 30°E, consistent with being in category PN. The faster-moving lower-frequency wave accumulates there with unbounded wavenumber and energy near 5°E, the zero-wind point, after a slight overshoot, as in category Pn.

In the strong westerlies at 210°E there are R1-E waves with the two periods (Fig. 7b). Their group velocities (Fig. 7c) drop to near zero in the weak westerlies at 280°E and their wavenumbers (Fig. 7d) and energies (Fig. 7e) both become very large there. Similar category Pp behavior is found for R1-E waves initiated in the Atlantic westerlies at 330°E. R1 waves cannot exist in the strong westerlies. Experiments indicate that in weaker westerlies (half of the U shown in Fig. 7a), ray paths of R1 waves with longer period and large h_e (e.g., 20 days and 500 m) can exist and are characteristic of category Np, with maximum energy and minimum wavenumber in maximum westerly around 235°E (not shown).

5. Relevance to observed wave climatologies

The observed winter and summer zonal winds in a vertical section on the equator are shown in Fig. 8a. The question addressed in this section is whether the observed distribution of equatorial waves may be determined to a significant extent by propagation on the varying upper-tropospheric zonal flow and
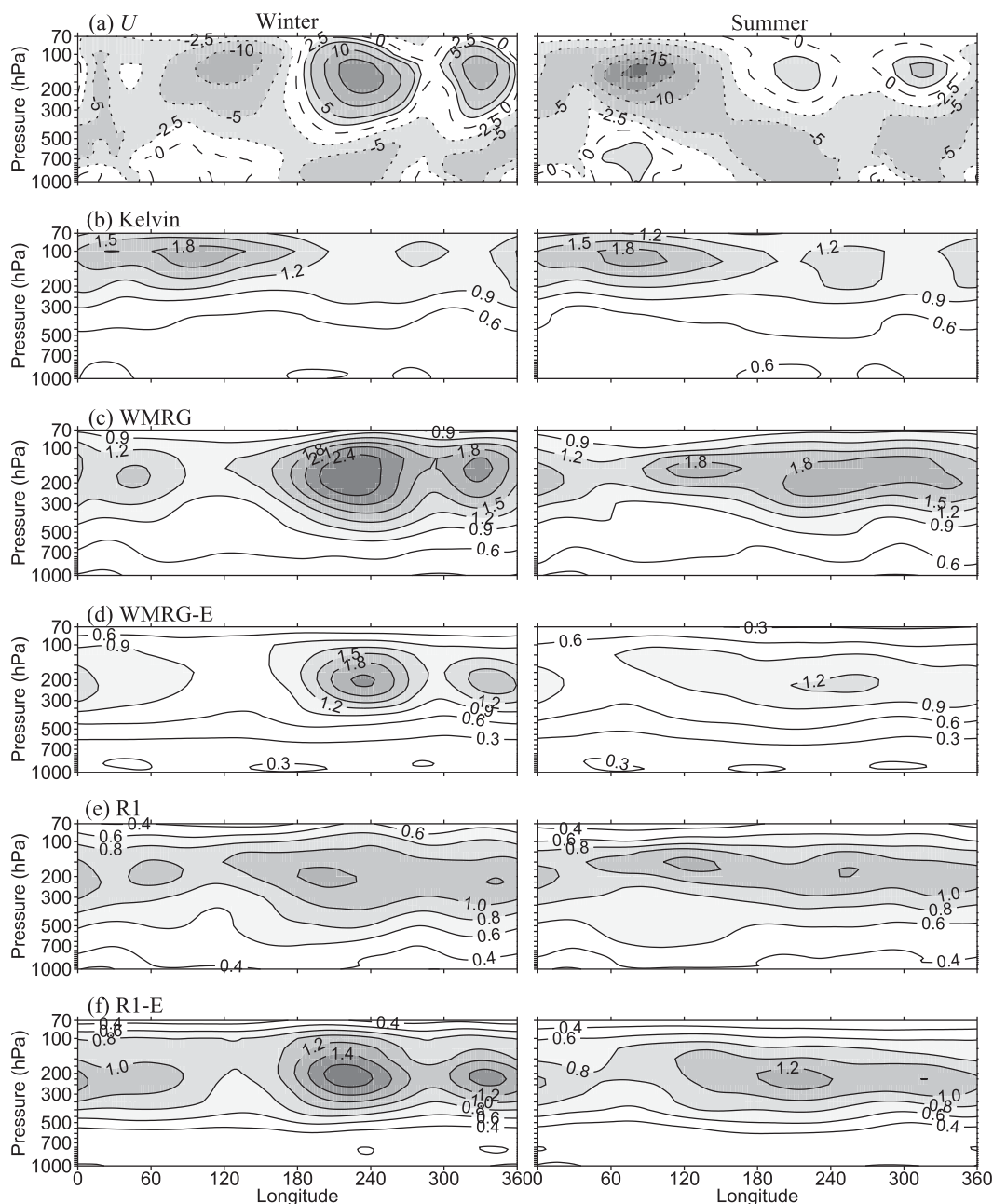
FIG. 8. Longitude–height cross section of equatorial zonal wind U and equatorial wave amplitudes in the domain $k = 2$–10 and period = 2–30 days for climatological (left) winter and (right) summer seasons. (a) Zonal wind averaged between 7°S and 7°N. The contour interval is 5 m s^{-1} except that ±2.5 is also drawn, with the positive contours solid, the zero contour dashed, and negative contours dotted. (b)–(f) The amplitudes of the various waves, measured by the standard deviation of (b) Kelvin wave u on the equator, (c) WMRG and (d) WMRG-E v on the equator, and (e) R1 and (f) R1-E v at 8°N. The contour intervals are 0.3 for the Kelvin and WMRG(-E) modes and 0.2 for the R1(-E) modes. The unit throughout is meters per second.

therefore be described by the analysis in this paper, or whether the distribution is dominated by other factors.

To split the near equatorial varying flow into equatorial wave components, the technique developed and used in Yang et al. (2003, 2007a, 2012) will be employed.

This technique is fully discussed in those papers. In brief, it involves splitting the transient motion into westward- and eastward-moving components and retaining only periods 2–30 days and wavenumbers 2–10. The fields are projected separately onto the equatorial wave mode
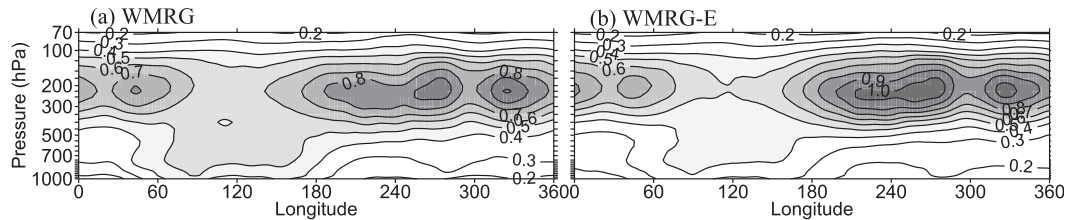
FIG. 9. Wave amplitudes for (a) WMRG and (b) WMRG-E waves in winter, as in Fig. 8, but for shorter waves with $k = 11$–30. The contour interval is one-third of that in Fig. 8.

structures with a latitudinal scale set by overall goodness of fit. This is done separately at each level. There is no assumption about the vertical structure or imposition of the dispersion relation. The standard deviations of the amplitudes of the gravest modes in the two seasons are shown as a function of longitude and height in Fig. 8. It is clear that upper-tropospheric amplitudes dominate and the extent to which propagation on the varying upper-tropospheric flow may explain them will now be discussed.

In both seasons, the Kelvin wave amplitudes (Fig. 8b) are largest in the easterly maximum in the EH and have a secondary maximum in the WH westerly flow minimum. This is consistent with Kelvin wave being in category PP and the computed wave energy shown in Fig. 3. In the winter the E Pacific and Atlantic westerlies are strong and between them there are weak westerlies. Correspondingly, the secondary maximum in Kelvin wave energy is weak and isolated. In the summer the westerly maxima are much weaker and there are weak easterlies between them, and the Kelvin wave secondary maximum is broader. Such details also appear to be consistent with equatorial propagation on a zonally varying upper-tropospheric flow being important in the observed Kelvin wave distribution.

The story is mostly very different for the WMRG(-E) and R1(-E) waves in winter. WMRG, WMRG-E, and R1-E are dominated by their amplitudes in the eastern Pacific and Atlantic westerly regions (Figs. 8c,d,f, left column). This is inconsistent with the distribution being dominated by propagation. According to this, the WMRG waves should be in category PP with maximum amplitude in the region between the westerlies, and WMRG-E and R1-E in category Pp should peak on the western flank of this, contrary to observation. Theory gives that and R1 waves energy should generally have an EH maximum in the weakest easterlies near 60°E (category PN), and the observed distribution does show this. Theory also gives that only low-frequency R1 waves can exist in the strong WH westerlies (Fig. 4h). The observed R1 distribution in the WH, which is dominated by a broad maximum with weak maxima in the westerly wind regions, is not consistent with the typical category

Pn. However, it could be consistent with category Np, which, as discussed in section 4e, can exist for R1 waves with very low frequency and large h_e when westerly is weak.

There is more agreement with the expectations from 1D propagation theory in summer (Fig. 8, right column). WMRG, WMRG-E, and R1 show maxima between the westerly maxima in the WH (category Pp). However, the distribution of R1-E is not clearly related to the theory.

The standard deviations in the high-wavenumber band 11–30 have also been examined for evidence of cascades to higher wavenumbers. The distribution for R1 and R1-E (not shown) is generally very similar to that for the lower-wavenumber components. However, as seen in Fig. 9, WMRG and WMRG-E do show winter maxima shifted eastward toward the region between the two westerly ducts, giving evidence of some accumulation as the waves propagate into that region (category Pp).

The propagation theory that has been applied to equatorial waves takes account of the varying zonal flow. However, it takes no account of the varying of the meridional gradient in the ambient absolute vorticity with longitude, using β throughout. To examine the likely sensitivity of the propagation of WMRG and R1 waves to zonal variation in the vorticity gradient, the ray tracing has been repeated but with β divided by 2 in the EH where the vorticity gradient is generally small and multiplied by 2 in the WH where it is generally large. The wavenumber and energy results for MRG are shown in Figs. 10a and 10b, and those for R1 waves in Figs. 10c and 10d. Comparison with Figs. 6d,e and Figs. 7d,e, respectively, shows that the behavior with longitude is very similar, with only quantitative differences. The lack of sensitivity to the magnitude of the meridional vorticity gradient compared with that to the variations in the zonal flow suggests that it is indeed a good first approximation to neglect variations in the former compared with those in the latter as is done in the theory.

6. Concluding comments

To examine the possible importance of the zonal propagation on a varying upper-tropospheric zonal flow
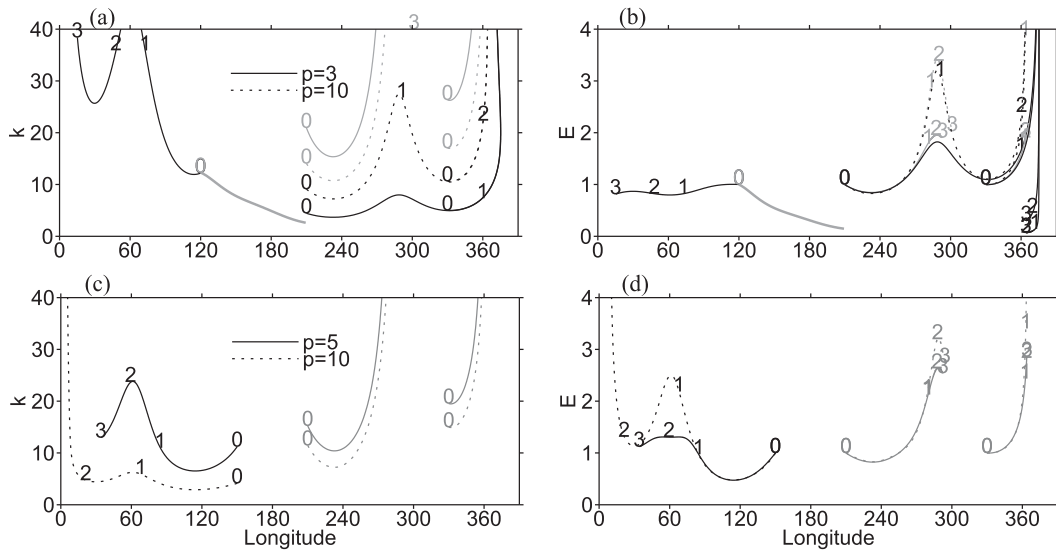
FIG. 10. Ray-tracing results for MRG and R1 waves with β reduced by a factor of 2 for starting points in the EH and multiplied by a factor of 2 for starting points in the WH. (a),(b) MRG k and E and (c),(d) R1 k and E. The conventions are as in Figs. 6 and 7.

for the climatological distribution of equatorial waves, the general theory for such 1D propagation has been developed from basic wave theory. Equations have been derived for the variation of wavenumber and wave energy along ray paths. Different categories of behavior are found, depending on the sign of the absolute group velocity and a parameter B that is a property of the wave in question and varies with its wavenumber. These categories have been illustrated schematically in Fig. 1. For positive B the wave energy and wavenumber behave in similar manners. For positive group velocity they both maximize in relative easterlies or on the western flank of them. In the latter case in which the group velocity tends to zero, this is the wave accumulation first discussed by Webster and Chang (1988). For negative group velocity the wavenumber and wave energy maxima are in the relative westerlies or become unbounded in accumulation on the eastern flanks of them.

However, if B is negative the behavior of the wave energy is opposite to that of the wavenumber. This is possible because the relevant conservation equation is for wave activity and not for wave energy. In this case, where k is a maximum, then E is a minimum and vice versa, and the concept of wave accumulation is not valid. The WMRG wave in weak easterlies is an example of a wave with B negative.

Applying the theory to equatorial waves, the nondispersive Kelvin wave has B a constant, 2, and analytic solutions for steady distributions of wave properties can be obtained. In particular for observed upper-tropospheric flows, there is maximum wave energy in

maximum easterly flow. There is a remarkably good agreement with the observed distribution of wave variance, suggesting that propagation on a varying flow is very important for these waves.

A general discussion of propagation of gravity, MRG, and R1 waves has been presented, with some important aspects illustrated by ray-tracing examples. In particular, it has been shown that in the EH WMRG waves would have maximum wave energy in the maxima in the easterlies, whereas R1 waves would maximize their wave energy in the minima in the easterlies. In the WH westerlies both WMRG and low-frequency R1 waves and their eastward-moving counterparts, WMRG-E and R1-E are possible. The wave energy in nearly all cases varies in the opposite sense of the basic flow, maximizing in the weak westerly region, or to the east of the westerly maximum. Comparison with the observed behavior has indeed shown some measure of consistency in the summer and in the EH in winter. However, in general there is little consistency with the winter distributions in the WH, these being dominated by maxima in the WH westerlies in the eastern Pacific and Atlantic.

Major assumptions have been made in the theory for propagation on a zonally varying flow and in its application to equatorial waves. These assumptions include consideration of only the upper-tropospheric zonal wind, using a climatological zonal flow with the implication of ignoring the large changes of the ambient zonal flow with, for example, ENSO, using a slowly varying approximation for the background flow and, consistent with this, a smoothed version of the zonal wind, and that 1D zonal

propagation is dominant. Given these rather drastic assumptions, the theory has been surprisingly successful in giving insight into the climatological distributions of Kelvin waves and some aspects of the other gravest waves.

However, there is a major inconsistency between the observed maxima of WMRG(-E) and R1-E wave amplitudes in the strong westerlies in the WH in winter and the predictions from the propagation theory. This is indicative of strong sources of these equatorial waves in the westerly regions, and, following Webster and Holton (1982) and subsequent research, is highly suggestive of the dominance in these westerly duct regions of forcing from higher latitudes. This relationship is examined in detail in Yang and Hoskins (2015, manuscript submitted to *Quart. J. Roy. Meteor. Soc.*). In this paper, the large variation in the strength of the westerly ducts with ENSO is used as a test bed for ideas on the mechanisms involved.

APPENDIX

Derivation of Equatorial Wave Mode Properties

The general expression for B is given in Eq. (10). This appendix gives the explicit expressions for B for each equatorial wave mode.

a. The Kelvin wave

As discussed in section 4a, the Kelvin wave has a nondispersive dispersion relation $\omega_i = c_e k$ and a group velocity $c_{gi} = c_i = c_e$, where $c_e = (gh)^{1/2}$ and h is the equivalent depth. In this case, Eq. (10) reduces to

$$B = 2. \tag{A1}$$

b. n = 0 EMRG and WMRG waves

For the $n = 0$ modes, the dispersion relation is

$$\omega_i = \frac{c_e}{2}[k \pm (k^2 + 4\beta/c_e)^{1/2}], \tag{A2}$$

where the upper sign is for EMRG waves and the lower sign for WMRG waves. Then

$$c_{gi} = \frac{\partial \omega_i}{\partial k} = \frac{c_e}{2}\left[1 \pm \frac{k}{(k^2 + 4\beta/c_e)^{1/2}}\right] \quad \text{and} \tag{A3}$$

$$\frac{\partial c_{gi}}{\partial k} = \pm \frac{2\beta}{(k^2 + 4\beta/c_e)^{3/2}}. \tag{A4}$$

Using Eqs. (A2)–(A4),

$$B = 1 \pm \frac{k}{(k^2 + 4\beta/c_e)^{1/2}} \mp \frac{2\beta k}{c_g(k^2 + 4\beta/c_e)^{3/2}}. \tag{A5}$$

c. n ≥ 1 equatorial Rossby and gravity waves

Equatorial $n \geq 1$ modes are divided into two classes: low-frequency Rossby waves and high-frequency gravity waves. Their dispersion relations are quite complicated. Therefore we will make use of the approximate forms given in Gill (1982).

1) EQUATORIAL ROSSBY WAVES

The Rossby wave dispersion relation is given approximately by

$$\omega_i = -\frac{\beta k}{k^2 + (2n + 1)\beta/c_e}. \tag{A6}$$

Then we have

$$c_{gi} = \frac{\beta[k^2 - (2n + 1)\beta/c_e]}{[k^2 + (2n + 1)\beta/c_e]^2} \quad \text{and} \tag{A7}$$

$$\frac{\partial c_{gi}}{\partial k} = -2\beta k \frac{k^2 - 3(2n + 1)\beta/c_e}{[k^2 + (2n + 1)\beta/c_e]^3}. \tag{A8}$$

Using Eqs. (A6)–(A8),

$$B = \frac{2(2n + 1)\beta/c_e}{k^2 + (2n + 1)\beta/c} + \frac{2\beta k^2}{c_g}\frac{[k^2 - 3(2n + 1)\beta/c_e]}{[k^2 + (2n + 1)\beta/c_e]^3}. \tag{A9}$$

2) EQUATORIAL GRAVITY WAVES

For gravity waves, their approximate dispersion relation is

$$\omega_i = \pm c_e[k^2 + (2n + 1)\beta/c_e]^{1/2}, \tag{A10}$$

with the upper sign for the eastward-moving and the lower sign for westward-moving waves. Then

$$c_{gi} = \pm \frac{kc_e}{[k^2 + (2n + 1)\beta/c_e]^{1/2}} \quad \text{and} \tag{A11}$$

$$\frac{\partial c_{gi}}{\partial k} = \pm \frac{(2n + 1)\beta}{[k^2 + (2n + 1)\beta/c_e]^{3/2}}. \tag{A12}$$

Using Eqs. (A10)–(A12),

$$B = 1 + \frac{k^2}{k^2 + (2n+1)\beta/c_e}$$
$$\mp \frac{(2n+1)\beta k}{c_g[k^2 + (2n+1)\beta/c_e]^{3/2}}. \tag{A13}$$

Equations (A1), (A5), (A9), and (A13) form a complete set of expressions for B for all equatorial wave modes.

REFERENCES

Bretherton, F. P, and C. J. R. Garrett, 1968: Wavetrains in inhomogeneous moving media. *Proc. Roy. Soc. London*, **302A**, 529–554, doi:10.1098/rspa.1968.0034.

Chang, H.-R., and P. J. Webster, 1995: Energy accumulation and emanation at low latitudes. Part III: Forward and backward accumulation. *J. Atmos. Sci.*, **52**, 2384–2403, doi:10.1175/1520-0469(1995)052<2384:EAAEAL>2.0.CO;2.

Dias, J., and G. N. Kiladis, 2014: Influence of the basic state zonal flow on convectively coupled equatorial waves. *Geophys. Res. Lett.*, **41**, 6904–6913, doi:10.1002/2014GL061476.

Gill, A. E., 1982: *Atmosphere–Ocean Dynamics*. Academic Press, 662 pp.

Hoskins, B. J., and G.-Y. Yang, 2000: The equatorial response to higher-latitude forcing. *J. Atmos. Sci.*, **57**, 1197–1213, doi:10.1175/1520-0469(2000)057<1197:TERTHL>2.0.CO;2.

Kiladis, G. N., and M. Wheeler, 1995: Horizontal and vertical structure of observed tropospheric equatorial Rossby waves. *J. Geophys. Res.*, **100**, 22 981–22 997, doi:10.1029/95JD02415.

Lighthill, J., 1978: *Waves in Fluid*. Cambridge University Press, 504 pp.

Tomas, R. A., and P. J. Webster, 1994: Horizontal and vertical structure of cross-equatorial wave propagation. *J. Atmos. Sci.*, **51**, 1417–1430, doi:10.1175/1520-0469(1994)051<1417:HAVSOC>2.0.CO;2.

Webster, P. J., and J. R. Holton, 1982: Cross-equatorial response to midlatitude forcing in a zonally varying basic state. *J. Atmos. Sci.*, **39**, 722–733, doi:10.1175/1520-0469(1982)039<0722:CERTML>2.0.CO;2.

——, and H.-R. Chang, 1988: Equatorial energy accumulation and emanation regions: Impacts of a zonally varying basic state. *J. Atmos. Sci.*, **45**, 803–829, doi:10.1175/1520-0469(1988)045<0803:EEAAER>2.0.CO;2.

Yang, G.-Y., and B. J. Hoskins, 2013: ENSO impact on Kelvin waves and associated tropical convection. *J. Atmos. Sci.*, **70**, 3513–3532, doi:10.1175/JAS-D-13-081.1.

——, ——, and J. M. Slingo, 2003: Convectively coupled equatorial waves: A new methodology for identifying wave structures in observational data. *J. Atmos. Sci.*, **60**, 1637–1654, doi:10.1175/1520-0469(2003)060<1637:CCEWAN>2.0.CO;2.

——, ——, and ——, 2007a: Convectively coupled equatorial waves. Part I: Horizontal structure. *J. Atmos. Sci.*, **64**, 3406–3423, doi:10.1175/JAS4017.1.

——, ——, and ——, 2007b: Convectively coupled equatorial waves. Part II: Zonal propagation. *J. Atmos. Sci.*, **64**, 3424–3437, doi:10.1175/JAS4018.1.

——, ——, and ——, 2007c: Convectively coupled equatorial waves. Part III: Synthesis structures and extratropical forcing. *J. Atmos. Sci.*, **64**, 3438–3451, doi:10.1175/JAS4019.1.

——, ——, and ——, 2011: Equatorial waves in opposite QBO phases. *J. Atmos. Sci.*, **68**, 839–862, doi:10.1175/2010JAS3514.1.

——, B. Hoskins, and L. Gray, 2012: The influence of the QBO on the propagation of equatorial waves into the stratosphere. *J. Atmos. Sci.*, **69**, 2959–2982, doi:10.1175/JAS-D-11-0342.1.

Zhang, C., 1993: Laterally forced equatorial perturbations in a linear model. Part II: Mobile forcing. *J. Atmos. Sci.*, **50**, 807–821, doi:10.1175/1520-0469(1993)050<0807:LFEPIA>2.0.CO;2.